Vapor–Liquid Equilibria for Binary Mixtures of 1-Alcohols in Carbon Disulfide

Kevin McKelgue

Department of Chemical Engineering, City College of the City University of New York, New York, New York 10031

Erdogan Gulari*

Department of Chemical Engineering, The University of Michigan, Ann Arbor, Michigan 48109

Isothermal vapor–liquid equilibrium data are reported for the systems methanol/CS_2, ethanol/CS_2, 1-propanol/CS_2, 1-butanol/CS_2, and 1-pentanol/CS_2 at 30 °C. The experimental technique provided complete $P-x-y$ data which were tested and found to be thermodynamically consistent by two methods. Correlations of the data with several different expressions for the excess Gibbs energy showed that, for each system, the Wilson equation best represented the data. Analysis of the fitted Wilson interaction parameters indicates decreasing alcohol–alcohol interactions and increasing alcohol–CS_2 interactions as the length of the alcohol's hydrocarbon chain increases.

Introduction

In addition to their extensive use in distillation and other vapor–liquid operations, vapor–liquid equilibrium (VLE) data can be used to calculate the excess Gibbs free energy, G^E, of liquid solutions. With a knowledge of the dependence of G^E on concentration, it is possible to determine the activity, a_i, of each component as well as the quantity $(\partial \mu_i / \partial x_i)$, where μ_i is the chemical potential and x_i is the mole fraction of component i. This quantity arises frequently in theories of transport in liquid solutions (1–3) and is thus of considerable value in evaluating such theories.

Often VLE data to calculate $(\partial \mu_i / \partial x_i)$ are not available for systems of interest. This is particularly true for solutions in which the pure components have widely different vapor pressures. For such solutions, little VLE data exist because their primary usefulness is limited. Such data are however important as a means of calculating a_i and $(\partial \mu_i / \partial x_i)$.

In this paper, VLE data and values of G^E are presented for a homologous series of 1-alcohols (methanol to pentanol) in solution with carbon disulfide at 30 °C. Prior to this work, VLE data for these systems were limited to methanol/CS_2 and ethanol/CS_2 at 20 °C (4).

Experimental Section

Materials. The carbon disulfide used in this work was obtained from Mallinckrodt Co. and had a specified purity of 99.5% with a water content of approximately 0.5%. It was further purified by drying over type 3A molecular sieves (Davisson, Inc.) resulting in a final purity of 99.9% CS_2. The methanol, also obtained from Mallinckrodt Co., had a specified purity of 99.9% and a water content of less than 0.02% and was used without further purification. The remaining alcohols were supplied by Fluka A. G. with guaranteed purities of 99.5%. The only further purification was treatment with 3Å molecular sieves to remove water. All purities were verified by infrared spectroscopy.

Apparatus. The vapor–liquid equilibria measurements were made using a static method in which the vapor-phase compositions and pressures were determined by analysis of IR spectra

of the vapor phase. The sample cell used in this study is shown schematically in Figure 1. It consists of a cylindrical quartz tube, 5 cm in length, which is sealed at each end with Infrasil quartz windows, resulting in a total vapor volume of approximately 15 cm³. The cell is connected by wide-bore valves to a vacuum pump at one end and a 50-mL glass vessel containing the liquid sample at the other. The entire cell was mounted inside the sample compartment of a Digilab FTS 20/C-E Fourier transform infrared spectrometer, with the vapor-containing portion of the cell directly in the infrared beam. The temperature inside the sample compartment was monitored with precision thermistor probes, precise to better than ±0.01 °C, in both the cell wall and the nitrogen bath. The temperature was maintained at 30.0 ± 0.1 °C throughout the course of the experiments.

The experimental procedure consisted of placing a 50-mL liquid sample of known composition in the cell, evacuating the vapor space above the sample, sealing off the cell by closing valve B, and then opening valve A to allow the vapor to fill the cell. Several infrared spectra of the vapor phase were obtained and compared until it was determined that the system had reached equilibrium at which time a high signal to noise ratio spectra was obtained and stored digitally for subsequent analysis. A plot of vapor-phase composition vs. time for the system 0.08 mole fraction ethanol in CS_2 is shown in Figure 2. This figure is representative of the approach to equilibrium encountered during these experiments.

The advantages of using this technique over the more common distillation or recirculation methods are (1) the low cost and simplicity of construction and operation of the cell and (2) the high accuracy to which relatively low vapor-phase compositions can be determined. The major disadvantage to this method is the relatively long time, approximately 2 h, required for the sample to attain equilibrium.

Data Analysis. The experimental method outlined allows complete $P-x-y$ data to be obtained from the IR spectrum of the vapor in equilibrium with a liquid. The low pressures encountered, coupled with the relatively small volume of the vapor, resulted in the liquid-phase composition remaining unchanged to within ±0.05%. Analysis of the IR spectrum of the vapor provides the remaining $P-y$ data.

The Infrasil windows of the cell are transparent over the range from 4000 to 2200 cm⁻¹. In this region of the spectrum are absorbance peaks due to O–H bonds (ca. 3700 cm⁻¹), C–H bonds (ca. 2275 cm⁻¹), and C=S bonds (ca. 2275 cm⁻¹). The concentration of a component, C_i, in moles per unit volume can be determined from its IR spectrum by the Beer–Lambert law

$$A = \epsilon_i c_i d \qquad (1)$$

where A is the integrated absorbance of the IR peak, ϵ_i is the integral extinction coefficient of component i, and d is the path length of the cell. The areas under the O–H, C–H, and C=S absorbance peaks were determined by fitting Gaussian or Lorentzian line shapes to the digital spectra using a nonlinear least-squares method as previously described (5). The ex-
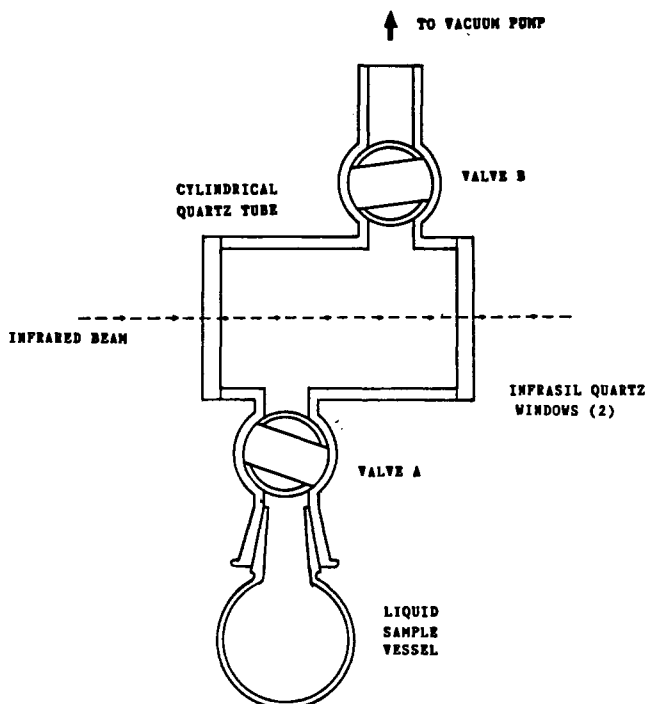
Figure 1. Schematic diagram of the infrared VLE cell used in this work.
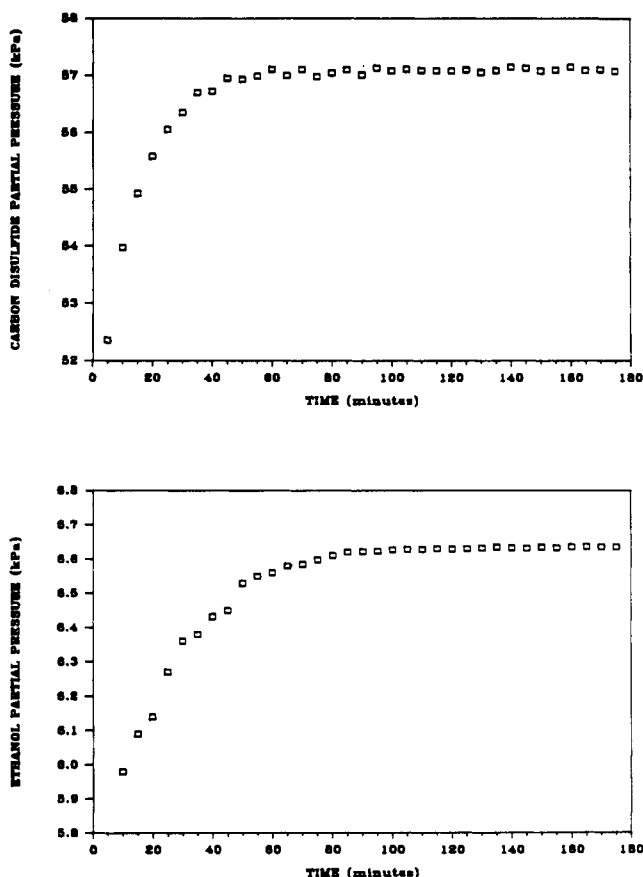

Figure 2. Concentration vs. time plot for the system 0.08 mole fraction ethanol in CS_2 showing the approach to equilibrium encountered during the experiments.

tinction coefficients for each component and peak were determined from measurements of the absorbance due to the pure component at its own vapor pressure, which was in turn measured by a precision (±0.03 kPa) mercury manometer. For these measurements, the pure component samples were first degassed under vacuum. The measured pure component va-

Table I. Experimental Data for the System Methanol (1)–Carbon Disulfide (2) at 30 °C

x_1	y_1	P, kPa	G^E/RT
0.001	0.022	60.3	0.0052
0.002	0.059	61.8	0.0103
0.005	0.118	65.5	0.0224
0.010	0.180	69.2	0.0426
0.020	0.216	73.4	0.0805
0.040	0.244	75.1	0.146
0.060	0.253	75.8	0.202
0.080	0.255	76.1	0.251
0.100	0.259	76.7	0.290
0.120	0.259	76.7	0.336
0.140	0.261	76.8	0.373
0.15	0.261	76.7	0.391

por pressures were found to agree to within ±2% with previously published values (4).

To determine the solution vapor pressures from the vapor-phase concentration data, an equation of state is needed. The relatively low partial pressures of alcohol in the vapor and the lack of any significant vapor-phase alcohol association allowed for the assumption of ideal behavior of the vapor phase. Because the frequency of the hydroxyl stretch is significantly shifted by hydrogen bonding (6), it would have been immediately apparent had there been significant vapor-phase alcohol self-association. The IR spectra obtained indicate that, with the exception of methanol, the degree of alcohol vapor-phase association was less than 0.5%. This degree of association would decrease the compressibility factor for the pure alcohol vapor to, at worst, no less than 0.995, justifying the assumption of vapor-phase ideality.

Only in the case of methanol was significant hydrogen bond mediated association observed in the IR spectrum of the pure component vapor. Thus, it was not possible to assume vapor-phase ideality for the methanol/CS_2 system. It should be noted that even though this system is expected to have the most nonideal vapor phase, the compressibility factor for methanol vapor at these conditions, calculated from published second and third virial coefficients (7), is 0.978. This value indicates that at the low pressures encountered, vapor-phase nonidealities due to association effects are actually quite small. Because the degree of association decreases rapidly with the length of the alcohol's hydrocarbon chain, the effect of association on the ideality of the vapor phase should be minimal for the other alcohols studied.

For the methanol/CS_2 system only, the vapor pressures of carefully degassed solutions were measured with a mercury manometer to an uncertainty of ±0.1 kPa. The compositions of the liquid phases were then determined by infrared spectroscopy. For the remaining alcohols, it was possible to compute the solution vapor pressure from the vapor-phase concentrations of alcohol and CS_2 by using the ideal gas law:

$$P = (C_{alcohol} + C_{CS_2})RT \tag{2}$$

This method was used to determine the vapor pressures for the ethanol/CS_2, 1-propanol/CS_2, 1-butanol/CS_2, and 1-pentanol/CS_2 systems to within ±0.05 kPa. Because the vapor pressures were calculated directly from measured absolute concentrations, the method is free from errors caused by the presence of small quantities of dissolved air in the liquid samples. Overall, the accuracy to which the vapor-phase compositions could be determined is approximately ±0.001 mole fraction over most of the concentration range. The liquid-phase mole fractions were also known to within ±0.001 mole fraction.

Results

The experimental data obtained are presented in Tables I–V. For the systems ethanol/CS_2, 1-propanol/CS_2, 1-butanol/CS_2, and 1-pentanol/CS_2, the data covers the entire concentration

Table II. Experimental Data for the System Ethanol (1)–Carbon Disulfide (2) at 30 °C.

equation	A_{12}	A_{21}	α_{12}	$\overline{\Delta\gamma_i}$	r^2
Margules	4.0022	−11.187		1.790	0.9731
van Laar	4.0277	0.68635		0.989	0.9898
Wilson	2114.7	511.74		0.208	0.9993
NRTL	921.86	2060.47	0.5895	0.476	0.9971
UNIQUAC	−250.98	1509.51		0.819	0.9928

x_1	y_1	P, kPa	G^E/RT
0.005	0.039	60.1	0.0178
0.010	0.058	61.2	0.0357
0.020	0.081	62.5	0.0691
0.040	0.097	63.5	0.129
0.080	0.104	63.7	0.228
0.120	0.113	63.7	0.302
0.180	0.117	63.5	0.384
0.300	0.120	63.0	0.477
0.400	0.126	61.5	0.511
0.500	0.132	61.2	0.512
0.700	0.154	56.2	0.409
0.850	0.218	44.0	0.242
0.900	0.272	36.7	0.171
0.950	0.377	25.8	0.091
0.980	0.598	17.4	0.0384
0.990	0.735	14.1	0.0193

Table III. Experimental Data for the System 1-Propanol (1)–Carbon Disulfide (2) at 30 °C

equation	A_{12}	A_{21}	α_{12}	$\overline{\Delta\gamma_i}$	r^2
Margules	2.6075	0.9396		0.432	0.9660
van Laar	2.6896	1.0198		0.229	0.9898
Wilson	1343.81	343.02		0.074	0.9982
NRTL	453.10	1360.42	0.6200	0.123	0.9951
UNIQUAC	−20.775	659.54		0.198	0.9918

x_1	y_1	P, kPa	G^E/RT
0.005	0.00441	57.9	0.0132
0.010	0.00783	57.9	0.0251
0.020	0.0126	57.8	0.0488
0.040	0.020	57.5	0.0925
0.080	0.029	56.8	0.167
0.120	0.032	56.4	0.226
0.180	0.35	55.7	0.293
0.300	0.038	54.1	0.370
0.500	0.048	49.7	0.386
0.700	0.069	40.3	0.296
0.850	0.117	27.0	0.170
0.900	0.158	20.6	0.118
0.950	0.267	12.9	0.0619
0.980	0.471	7.50	0.0255
0.990	0.638	5.61	0.129

Table IV. Experimental Data for the System 1-Butanol (1)–Carbon Disulfide (2) at 30 °C

equation	A_{12}	A_{21}	α_{12}	$\overline{\Delta\gamma_i}$	r^2
Margules	2.3410	0.5989		0.322	0.9694
van Laar	2.4260	0.8206		0.140	0.9938
Wilson	1184.83	300.93		0.092	0.9965
NRTL	238.76	1285.64	0.6207	0.095	0.9956
UNIQUAC	−13.566	511.08		0.134	0.9941

x_1	y_1	P, kPa	G^E/RT
0.005	0.00120	57.8	0.0121
0.010	0.00203	57.6	0.0221
0.020	0.00351	57.2	0.431
0.040	0.0063	56.5	0.0814
0.080	0.0076	55.5	0.146
0.120	0.0092	54.8	0.197
0.180	0.0104	54.0	0.252
0.300	0.0122	51.6	0.310
0.500	0.0170	45.0	0.311
0.700	0.0271	33.4	0.230
0.850	0.0544	20.1	0.130
0.900	0.0793	14.5	0.0901
0.950	0.142	8.30	0.470
0.980	0.289	4.15	0.0193
0.990	0.460	2.72	0.0097

Table V. Experimental Data for the System 1-Pentanol (1)–Carbon Disulfide (2) at 30 °C

equation	A_{12}	A_{21}	α_{12}	$\overline{\Delta\gamma_i}$	r^2
Margules	2.0753	0.2225		0.278	0.9543
van Laar	2.1957	0.5579		0.088	0.9958
Wilson	1055.63	202.48		0.044	0.9979
NRTL	171.76	1195.27	0.7946	0.058	0.9975
UNIQUAC	−79.74	459.23		0.093	0.9952

x_1	y_1	P, kPa	G^E/RT
0.005	0.00031	57.7	0.0096
0.010	0.00063	57.5	0.0195
0.020	0.0011	57.0	0.0378
0.040	0.0016	56.4	0.709
0.080	0.0023	55.3	0.125
0.120	0.0027	54.4	0.167
0.180	0.0032	53.0	0.210
0.300	0.0041	49.9	0.250
0.500	0.0065	41.4	0.242
0.700	0.0121	28.8	0.173
0.850	0.026	16.0	0.0951
0.900	0.037	11.2	0.0655
0.950	0.078	5.99	0.0340
0.980	0.173	2.72	0.0140
0.990	0.295	1.67	0.0071

range from $x_1 = 0$ to $x_1 = 1$. In the case of methanol/CS$_2$, data are presented only over the range from $x_1 = 0$ to $x_1 = 0.15$. Slightly beyond this concentration, the solution was observed to separate into two liquid phases. We previously reported a phase diagram for the methanol/CS$_2$ system (8) which indicated an upper consolute temperature of 36.1 °C.

In Table II it can be observed from the x–y data that the ethanol/CS$_2$ system forms an azeotrope at some point between $x_1 = 0.08$ and $x_1 = 0.12$. Using linear interpolation to estimate the composition of the azeotrope yielded a value of $x_1 = 0.111$. None of the other systems were found to be azeotropic.

The excess Gibbs free energy, G^E, was calculated from the P–x–y data by using

$$G^E = (x_1 \ln \gamma_1 + x_2 \ln \gamma_2)RT \tag{3}$$

$$\gamma_i = (y_iP)/(x_iP_i{}^{sat}) \tag{4}$$

where vapor-phase ideality has been assumed in the calculation of the activity coefficients, γ_i. Calculated values of G^E/RT for each data point are also given in Tables I–V.

As verification of the validity and overall accuracy of the experimental technique employed, the data obtained for the ethanol/CS$_2$ system are compared in Figures 3 and 4 with data previously reported in the literature (4). The present data were obtained at 30.0 °C while the literature data were for 20.0 °C. To allow comparison of VLE data at different temperatures, a solution theory must be used. As the Wilson equation was found to best represent the present data, it was used to obtain a correction factor to adjust the data to 20.0 °C. In doing this it was assumed that the Wilson interaction parameters for the system $(\lambda_{12} - \lambda_{11})$ and $(\lambda_{12} - \lambda_{22})$ remained constant over the 10 °C temperature interval.

The Wilson parameters obtained from a fit to the 30 °C data were used to determine the values of the activity coefficients predicted by the Wilson equation at 20 and 30 °C, γ_i (Wilson, 20 °C) and γ_i (Wilson, 30 °C). These values were then used to obtain the desired correction factor:

$$\gamma_i(20\ °C,\ cor) = \gamma_i(30\ °C,\ exptl)\left(\frac{\gamma_i(\text{Wilson, 20 °C})}{\gamma_i(\text{Wilson, 30 °C})}\right) \tag{5}$$
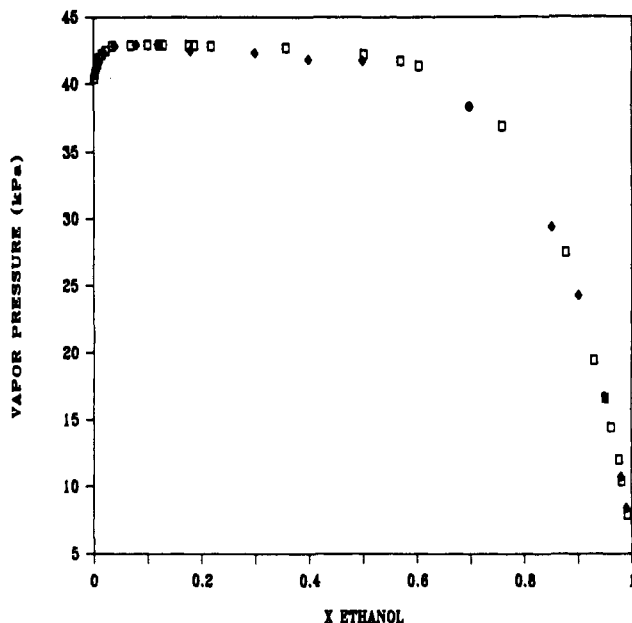
Figure 3. Vapor pressure vs. mole fraction of ethanol for the system ethanol/CS$_2$: ($\blacklozenge$) this work, ($\square$) taken from ref 4.
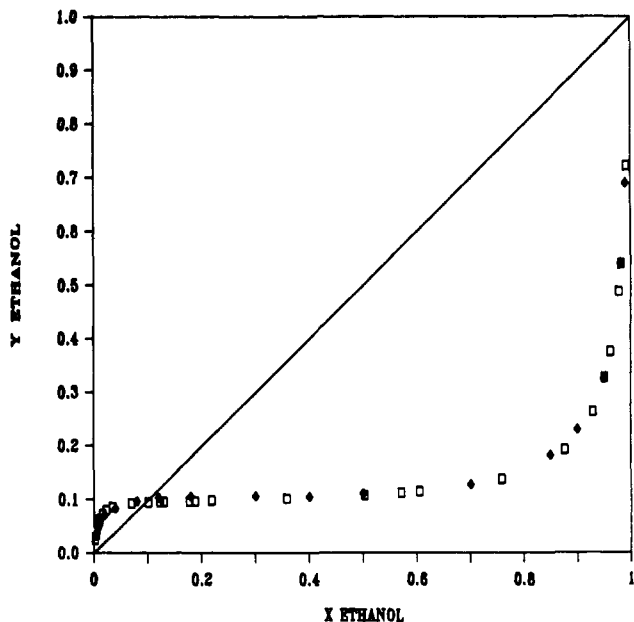
Figure 4. X-Y diagram for the system ethanol/CS$_2$: ($\blacklozenge$) this work, ($\square$) taken from ref 4.

This method corrects the data to 20 °C while maintaining the scatter in the experimental data. From these corrected activity coefficients and published Antoine equation coefficients (4) P-x-y data at 20 °C were obtained.

In Figure 3 the comparison between the data sets is made on P-x coordinates and in Figure 4 the x-y data are compared. In both cases, the two data sets are found to lie along the same curve to within experimental uncertainty.

The thermodynamic consistency of the data was verified using two methods: the integral test (9) and the point-to-point test developed by Van Ness et al. (10) and Christiansen and Fredenslund (11). For the latter method, fourth-order Legendre polynomials, with coefficients optimized by a least-squares procedure were used to represent G^E/RT as a function of x$_1$. The results of both tests are summarized in Table VI. The values reported for the integral test are the relative differences in the area above and below the x$_1$ axis in a plot of ln (γ_1/γ_2) vs. x$_1$. Because of the limited range of experimental data for

Table VI. Thermodynamic Consistency Analysis

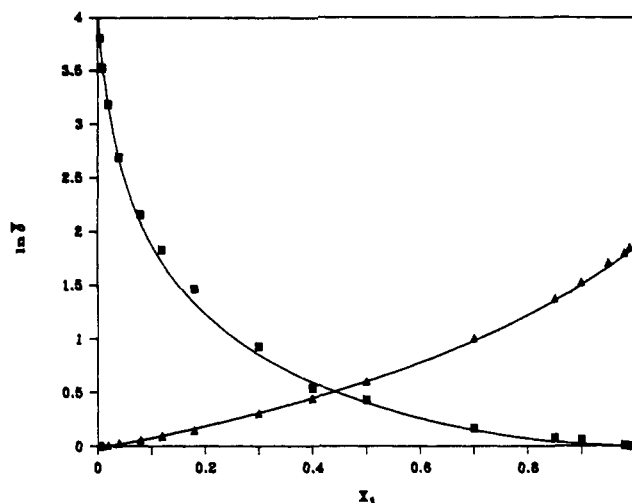| system	integral test (% diff)	point test (Δy_1)
methanol/CS$_2$		0.0034
ethanol/CS$_2$	1.92	0.0075
1-propanol/CS$_2$	1.68	0.0011
1-butanol/CS$_2$	1.54	0.0020
1-pentanol/CS$_2$	2.43	0.0009

Figure 5. Activity coefficients vs. mole fraction of ethanol for the system ethanol (1)/CS$_2$ (2) at 30 °C. The line indicates the fit of the Wilson equation to the data.

the methanol/CS$_2$ system, it was not possible to test that set of data using the integral method. For the point-to-point test, the mean difference between the measured and calculated values of y$_1$ is given (10). These results indicate, according to the criteria suggested by Gmehling et al. (4), that each set of data is thermodynamically consistent.

Tables II-V also show the results of fitting the experimental data to the Margules (12), van Laar (13), Wilson (14), NRTL (15), and UNIQUAC (16) equations. In fitting the parameters, the pure component properties and Antoine coefficients given by Gmehling et al. (4) were used. The objective function, F, minimized in the fitting procedure is given in eq 6. In Tables

$$F = \sum_{i=1}^{N}\sum_{j=1}^{2}\left(\frac{\gamma_{iJ,\text{exptl}} - \gamma_{iJ,\text{calcd}}}{\gamma_{iJ,\text{exptl}}}\right)^2 \tag{6}$$

II-V the coefficients A$_{ij}$ have their usual meaning in the Margules and van Laar equations and are used to represent the quantity ($\lambda_{ij} - \lambda_{jj}$) in the Wilson equation, (g$_{ij}$ - g$_{jj}$) in the NRTL equation, and (u$_{ij}$ - u$_{jj}$) in the UNIQUAC equation. For these three interaction parameter quantities, A$_{ij}$ is given in units of cal/mol.

For each system, both the mean deviation in the activity coefficients, $\overline{\Delta\gamma_i}$, defined by eq 7, and the square of the cor-

$$\overline{\Delta\gamma_i} = \frac{1}{2N}\sum_{i=1}^{N}\sum_{j=1}^{2}\left|\frac{\gamma_{iJ,\text{exptl}} - \gamma_{iJ,\text{calcd}}}{\gamma_{iJ,\text{exptl}}}\right| \tag{7}$$

relation coefficient, r^2, can be used to compare the quality of fit for the five different equations. The values of $\overline{\Delta\gamma_i}$ and r^2 given in Tables II-V indicate that for each system, the van Laar, Wilson, NRTL, and UNIQUAC equations represent the data fairly well. However, the Wilson equation provides a slightly better fit in all cases. It should be pointed out that the
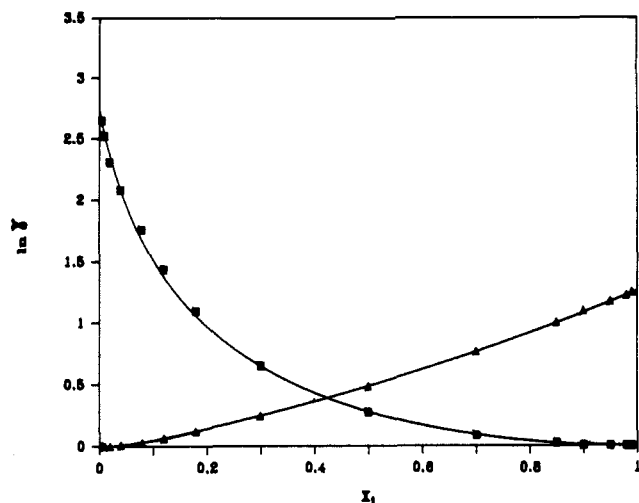
Figure 6. Activity coefficients vs. mole fraction of propanol for the system 1-propanol (1)/CS_2 (2) at 30 °C. The line indicates the fit of the Wilson equation to the data.
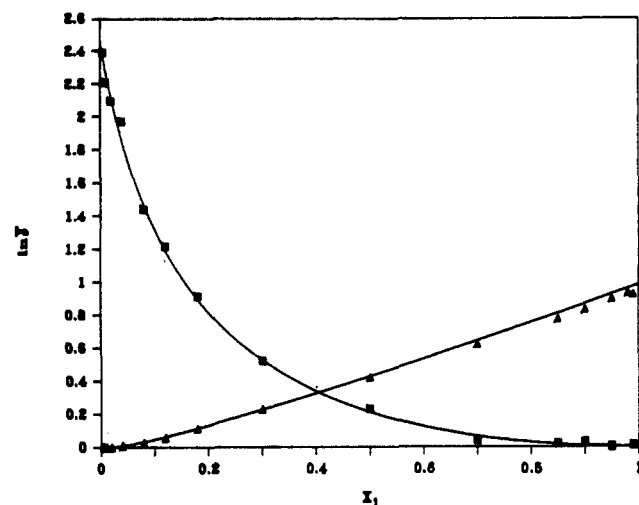

Figure 7. Activity coefficients vs. mole fraction of butanol for the system 1-butanol (1)/CS_2 (2) at 30 °C. The line indicates the fit of the Wilson equation to the data.

surprisingly large value of $\overline{\Delta\gamma_i}$ for the ethanol/CS_2 system is merely a result of the very large values of γ_1 for this system at low alcohol concentrations (γ_1^∞ = 58.2 using the Wilson equation).

The fit of the experimental data to the Wilson equation is actually quite good, as shown in Figures 5–8 where the experimental and calculated values of γ_1 and γ_2 are plotted against concentration for each system. This behavior is similar to that observed in numerous other alcohol-containing systems where it is often found that the Wilson equation well represents the experimental data.

The λ's in the Wilson equation are essentially negative interaction energy parameters gauging the attraction between the type molecules indicated by the subscripts (17). Although the values of the γ's themselves are inaccessible from an analysis of the VLE data, the Wilson parameters A_{12} and A_{21} provide values for functions of the λ's from which useful information can be obtained. As A_{12} is equal to $\lambda_{12} - \lambda_{11}$, the larger the A_{12} is, the greater the alcohol-alcohol attraction is over the alcohol-CS_2 interaction. Similarly, the larger the A_{21} is, the greater the CS_2-CS_2 attraction is over the alcohol-CS_2 attraction. The difference between A_{12} and A_{21}, $\lambda_{22} - \lambda_{11}$, can provide the most information. The larger the value of $\lambda_{22} - \lambda_{11}$ is, the greater the alcohol-alcohol attraction is over the CS_2-CS_2 interaction. As direct CS_2-CS_2 interactions remain con-
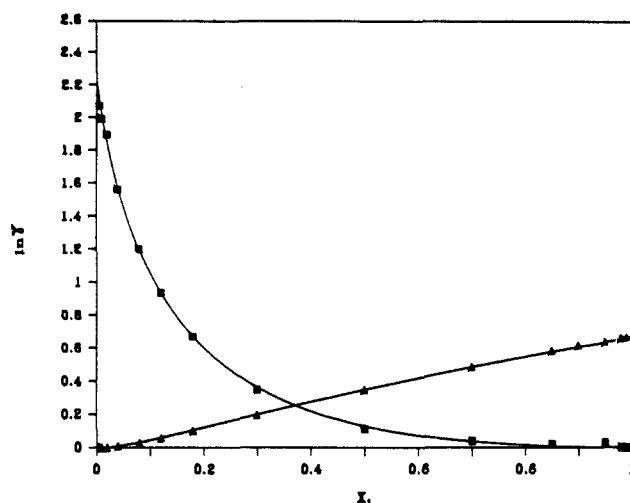
Figure 8. Activity coefficients vs. mole fraction of pentanol for the system 1-pentanol (1)/CS_2 (2) at 30 °C. The line indicates the fit of the Wilson equation to the data.

Table VII. Wilson Parameters $\lambda_{12} - \lambda_{11}$ and $\lambda_{12} - \lambda_{22}$ and Their Difference for Each System

system	$\lambda_{12} - \lambda_{11}$	$\lambda_{12} - \lambda_{22}$	$\lambda_{22} - \lambda_{11}$
ethanol/CS_2	2115	512	1603
1-propanol/CS_2	1344	343	1001
1-butanol/CS_2	1184	300	884
1-pentanol/CS_2	1055	202	853

stant regardless of the type of alcohol present, this term provides a measure of the relative strength of alcohol-alcohol interactions over the homologous series.

Table VII gives the values of $\lambda_{12} - \lambda_{11}$, $\lambda_{12} - \lambda_{22}$, and $\lambda_{22} - \lambda_{11}$ for each system. The decrease in the value of $\lambda_{22} - \lambda_{11}$ with increasing hydrocarbon chain length indicates decreasing attraction between the alcohol molecules. Similarly, the decline of $\lambda_{12} - \lambda_{22}$ with chain length reveals an increasing attraction between the CS_2 and alcohol molecules. This trend is expected and is in agreement with that observed by Wolff and Shadlakhy (18) for the homologous series of 1-alcohols in n-hexane.

Glossary

a_i	activity of component i
A	integrated absorbance of IR peak
A_{ij}	parameters in Margules, van Laar, Wilson, NRTL, and UNIQUAC equations
C_i	concentration of component i
d	path length of IR cell
F	objective function
g_{ij}	interaction parameter in NRTL equation
G^E	excess Gibbs free energy
N	number of data points
P	pressure
P_i^{sat}	vapor pressure of component i
R	gas constant
T	absolute temperature
u_{ij}	interaction parameter in UNIQUAC equation
x_i	mole fraction of i in liquid phase
y_i	mole fraction of i in vapor phase

Greek Letters

α_{ij}	nonrandomness parameter in NRTL equation
γ_i	activity coefficient of component i
ϵ_i	extinction coefficient of component i
λ_{ij}	interaction parameter in Wilson equation
μ_i	chemical potential of i

Literature Cited

(1) Kirkwood, J. G.; Baldwin, R. L.; Dunlop, P. J.; Gosting, L. J.; Kegeles, G. J. Chem. Phys. 1960, 33, 1505.
(2) de Groot, S. R.; Mazur, P. Non-Equilibrium Thermodynamics; North-Holland: Amsterdam, 1962.
(3) Fitts, D. D. Non-Equilibrium Thermodynamics; McGraw-Hill: New York, 1962.
(4) Gmehling, J.; Onken, U. Vapor-Liquid Equilibrium Data Collection; DECHEMA Chemistry Data Series: Frankfurt, 1977; Vol. I.
(5) McKeigue, K. Ph.D. Thesis, The University of Michigan, 1985.
(6) Schuster, P.; Zundel, G.; Sandorfy, C. The Hydrogen Bond; North-Holland: Amsterdam, 1976.
(7) Chang, E.; Cataldo, J. C. G.; Streett, W. B. J. Chem. Eng. Data 1982, 27, 293.
(8) McKeigue, K.; Gulari, E. J. Phys. Chem. 1984, 88, 3472.
(9) Redlich, O.; Kister, A. T. Ind. Eng. Chem. 1948, 40, 341.
(10) Van Ness, H. C.; Byers, S. M.; Gibbs, R. E. AIChE J. 1973, 19, 238.

(11) Christiansen, L. J.; Fredenslund, A. AIChE J. 1975, 21, 49.
(12) Margules, M. Sitzungsber. Akad. Wiss. Wien 1985, 104j, 1243.
(13) van Laar, J. J. Z. Phys. Chem. 1910, 72, 723.
(14) Wilson, G. M. J. Am. Chem. Soc. 1964, 86, 127.
(15) Renon, H.; Prausnitz, J. M. AIChE J. 1968, 14, 135.
(16) Abrams, D. S.; Prausnitz, J. M. AIChE J. 1975, 21, 116.
(17) Prausnitz, J. M. Molecular Thermodynamics of Fluid Phase Equilibria; Prentice-Hall: Englewood Cliffs, NJ, 1969.
(18) Wolff, H.; Shadiakhy, A. Fluid Phase Equilibria 1981, 7, 309.

Solubilities of Ammonium Iodide, Ammonium Bromide, and Ammonium Iodide–Ammonium Bromide Mixture in Liquid Ammonia

Hideki Yamamoto,* Junji Tokunaga, and Seiji Sanga

Department of Chemical Engineering, Faculty of Engineering, Kansai University, Osaka, 564, Japan

Solubilities of ammonium iodide and ammonium bromide in liquid ammonia were determined in the temperature range 270.0–350.0 K. Solubilities of these solutes in liquid ammonia increased with the temperature, and the values of weight percent solubility increased from 77.34 to 83.01 wt % for ammonium iodide, and from 88.71 to 73.19 wt % for ammonium bromide. Solubilities of the mixtures of ammonium iodide and ammonium bromide (four weight ratios of NH_4I/NH_4Br = 0.37, 0.80, 1.48, and 2.95) in liquid ammonia were also determined in the temperature range 270.0–350.0 K. The relation between temperature and weight percent solubility for ammonium iodide in liquid ammonia was shown by a smooth curve, but a bend point appeared on the solubility curve for ammonium bromide or its mixture with ammonium iodide in liquid ammonia. With increasing weight ratios of ammonium iodide to ammonium bromide, the bend point on the solubility curve gradually moved toward lower temperature.

Introduction

The solubility data of ammonium halides in liquid ammonia are required both for the design of thermal energy storage system utilizing chemical reaction in liquid ammonia solution (1) and for the development of chemical heat pumps that use these solution systems (2).

The purpose of this work is to obtain experimental data for the solubility of ammonium iodide, ammonium bromide, and ammonium iodide–ammonium bromide mixture in liquid ammonia in the temperature range 270.0–350.0 K.

The solubility data for pure ammonium halides in liquid ammonia were reported at 298 K by Hunt (3, 4), and at several temperatures by Kendall and Davidson (5). Solubilities in a wider temperature range, however, have not yet been reported. No data for the solubility of ammonium iodide–ammonium bromide mixture in liquid ammonia are available.

Experimental Section

Materials. Ammonium iodide (NH_4I) and ammonium bromide (NH_4Br) from Wako Junyaku Co. Ltd. were of guaranteed reagent grade and were specified as the pure grade having minimum purities of 99.5% and used without further purification. The powdered crystal was thoroughly dried at 373 K and stored over silica gel in a desiccator.

Ammonia gas of 99.99% purity was provided from Seitetu Kagaku Co. Ltd.

Expression of Solubility. The solubility is presented in weight percent. Weight percent is here defined as the ratio of the mass of solute to that of solution; that is,

$$X = \frac{100S}{S + Vd_1} \tag{1}$$

where X is the weight percent solubility, S is the weight of solute dissolved in liquid ammonia, V is the volume of liquid ammonia, and d_1 is the density of liquid ammonia.

Experimental Apparatus. The schematic diagram of the experimental apparatus is shown in Figure 1. The two vessels (I and J) are made of pressure-resistant glass (up to 2 MPa); one is a 20-mL vessel for measuring the volume of liquid ammonia, and the other is a 100-mL vessel for determining the solubility that can be agitated by a magnetic stirrer (B).

These two vessels were immersed in a constant-temperature water bath within 0.05 K. The temperature control of the bath was maintained by using a refrigeration unit combined with a electric relay unit and thermoregulator.

The temperature in the vessels was measured by chromel-alumel thermocouple (F) corrected by a standard mercury thermometer. The temperature in the vessels was regulated within 0.05 K.

The pressure of the liquid ammonia solution was measured by a strain gauge transducer (A) with an accuracy of 0.1% of full scale (2 MPa).

The volume of the solution and the liquid ammonia was measured by a cathetometer (L) within ±0.02% of full volume.